**Proceedings of ICFDP7:**
**Seventh International Conference Of Fluid Dynamics And Propulsion**
**Dec. 18-20, 2001, Cairo, EGYPT**

# ICFDP7-2001071

# THE EFFECTS OF SYSTEM ROTATION WITH THREE ORTHOGONAL ROTATING AXES ON TURBULENT CHANNEL FLOW

Osama A. El-Samni
Department of Mechanical Engineering
The University of Tokyo
Hongo 7-3-1, Bunkyo-ku
Tokyo 113-8656, Japan
Tel.: 03-5841-6419, Fax: 03-5800-6999
e-mail: elsamni@thtlab.t.u-tokyo.ac.jp

Nobuhide Kasagi
Department of Mechanical Engineering
The University of Tokyo
Hongo 7-3-1, Bunkyo-ku
Tokyo 113-8656, Japan
Tel.: 03-5841-6417, Fax: 03-5800-6999
e-mail: kasagi@thtlab.t.u-tokyo.ac.jp

*Keywords*: System rotation, turbulent channel flow, DNS, Coriolis effect.

## ABSTRACT

The effect of Coriolis force on turbulent channel flow has been sought in a more general manner by taking into account the alignment between the rotation axis and the direction of mean pressure gradient and the rotation rate as well. Three different, but orthogonal rotation vectors coincident with the Cartesian coordinates have been imposed on a plane channel, in which homogeneity is presumed in the planes parallel to the wall. A series of DNS has been performed for each case starting from the non-rotating plane channel, while increasing the rotation number and keeping the Reynolds number based on the friction velocity at 150. Detailed statistics are obtained including mean quantities, turbulent intensities, vorticities, and higher-order moments. The budgets of transport equations of the quantities relevant to turbulence modeling are prepared for the three orthogonal cases in order to help assessing turbulence models. An attempt to investigate the near-wall structures has been tried.

## INTRODUCTION

Turbulent rotating flows are of great practical importance in nature and in many industrial applications. In rotating machinery, such as pumps, compressors and gas turbines, great efforts have been directed towards exploring the transport phenomena inside the rotating passages in order to improve their performance. Coriolis and centrifugal forces affect fluid dynamics inside such rotating devices. The alignment of those body forces with respect to the bounded walls is believed to have a significant role in modifying flow structures. Various geometrical configurations are likely to exist in rotating machineries such as: rectangular ducts, pipes, U-bends, elbows, curved channels, etc., which make the flow more complicated due to the combined effect with Coriolis forces arisen from system rotation. Thus, a plane channel has been chosen in the present study in order to isolate the sole effect of Coriolis force. Moreover, the simplicity of plane channel computed with spectral methods enables changing the flow parameters, especially Reynolds and rotation numbers, and also the orientation of the rotation vector much easier than corresponding experimental setups.

Turbulent channel flow subjected to system rotation has been studied experimentally and numerically for three decades since the experimental work of Johnston et al. [1], who observed the stabilization of turbulent flow near the leading (suction) wall and the augmentation of turbulence near the trailing (pressure) wall in a spanwise rotating channel. Kim [2] used LES to study the effect of spanwise rotation and reproduced most of the observations in the experiments. Kristoffersen and Andersson [3] used DNS to study the effect of spanwise rotation using a finite difference algorithm with the rotation number, based on the friction velocity, up to 7.6 and their detailed turbulence statistics were reported by Andersson and Kristoffersen [4]. Recently, Oberlack et al. [5] studied streamwise system rotation using DNS, LES and turbulence models. The rotation numbers of 3.2 and 10 were tested in their simulations for the purpose of verifying the similarity theory. Detailed information about the flow structures have not been addressed. The present study aims at exploring the general effect of system rotation on wall-bounded flows by testing three orthogonal cases independently. The rotation number has been increased to include the ranges deduced from the conceptual design of small-scale gas turbine. Emphasis is laid upon comparing statistics, budgets and flow structures in different orientations and also with their values in non-rotating channel.

## NOMENCLATURE

| | |
|---|---|
| $a_1$ | structure parameter |
| $C_f$ | friction coefficient, $C_f = 2\tau_w / \rho U_b^2$ |
| $D_k$ | viscous diffusion of $k$ |
| $F$ | flatness factor |
| $k$ | turbulent kinetic energy |
| $P_k$ | mean production of $k$ |
| $Re_\tau$ | Reynolds number, $Re_\tau = u_\tau \delta / \nu$ |
| $Ro_\tau$ | Rotation number, $Ro_\tau = 2\delta\Omega / u_\tau$ |
| $S$ | skewness factor |
| $S_{ij}$ | symmetric part of the strain rate tensor $(u_{i,j} + u_{j,i})/2$ |
| $T_k$ | turbulent transport rate of $k$ |
| $U, W$ | mean velocities in $x$-and $z$-directions |
| $U_b$ | bulk velocity |
| $u, v, w$ | fluctuating velocities in $x$-, $y$- and $z$-directions |
| $u_\tau$ | friction velocity |
| $u_\tau^*$ | friction velocity based on the total shear at both walls |
| $x, y, z$ | streamwise, wall-normal and spanwise directions |

### *Greek symbols and superscripts*

| | |
|---|---|
| $\delta$ | channel half width |
| $\gamma_m, \gamma_g$ | Mean flow and gradient angles |
| $\varepsilon_k$ | dissipation rate of $k$ |
| $\Pi_k$ | pressure diffusion of $k$ |
| $-\lambda_2$ | second largest eigenvalue of the tensor $S_{ik}S_{kj} + \Omega_{ik}\Omega_{kj}$ |
| $\nu$ | kinematic viscosity |
| $\tau_w$ | wall shear stress |
| $\tau_w^*$ | modified wall shear stress in Case WN |
| $\Omega$ | angular velocity of system rotation |
| $\Omega_{ij}$ | anti-symmetric part of the strain rate tensor $(u_{i,j} - u_{j,i})/2$ |
| $\omega_i$ | vorticity component in $i^{th}$–direction |
| $+$ | normalized by local friction velocity $u_\tau$ and $\nu$ |
| $*$ | normalized by friction velocity $u_\tau^*$ and $\nu$ |

## COMPUTATIONAL DETAILS

Three different cases, each of which corresponds to a different rotation vector, are tested. Cases SP, ST and WN correspond to the rotation around the spanwise, streamwise and wall-normal axes, respectively. A sketch of the computational domain is shown in Fig. 1. The rotation number $Ro_\tau = 2\Omega\delta / u_\tau$ has been increased up to 15 in Cases SP & ST. In Case WN, the maximum rotation number studied is 0.04. Five intermediate rotation cases of $Ro_\tau$ = 2.5, 5, 7.5, 11 and 15 were studied in Cases SP & ST, while only three intermediate rotation numbers of 0.01, 0.02 and 0.04 were preformed in Case WN. These ranges cover real conditions deduced from a conceptual design of small gas turbines of 30-100 kW [6]. A fully developed flow is established with periodic boundary conditions in the streamwise and spanwise directions. The driving pressure gradient is adjusted to keep the mass flow rate in the $x$-direction always constant in all simulation, and the bulk Reynolds number, $U_b\delta/\nu$, remains at 2265. The computations in each orthogonal case have been started from the initial data of non-rotating channel using coarse grids of $64 \times 65 \times 64$ in the $x$-, $y$-, and $z$-directions, respectively. Such coarse-grid computations help in providing the common features of low-order statistics, which are affected by system rotation.

Higher-order statistics and the budgets of the transport equations are generated for only the highest rotation number in each case using finer grids of 128×129×128 in Cases SP & ST and of 192×129×128 in Case WN. The computational domain has lengths of $5\pi\delta \times 2\delta \times 2\pi\delta$ in the $x$-, $y$-, and $z$-directions, respectively. The variables have been non-dimensionalized by the channel half width $\delta$, friction velocity $u_\tau$. The time step in fine grid simulations is in range of 0.045 - 0.06 $u_\tau^2/\nu$ to keep the Courant number less than 0.3 in all studied cases. Further details about the numerical techniques and the sampling procedures are referred to El-Samni [7].

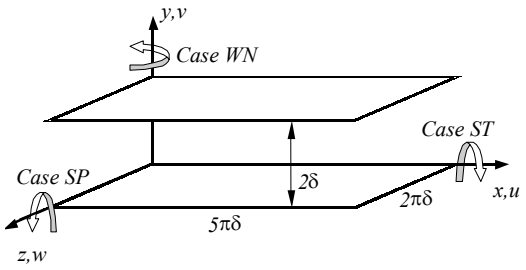


Figure 1 computational domain of rotating channel

## MEAN VELOCITIES

In Case SP, asymmetric profiles of the mean velocity in the $x$-direction with a linear slope of twice the rotation speed in the central region of the channel are recaptured well in the coarse-grid simulations as shown in Fig. 2(a). Note that the statistical quantities in Case SP, presented here, are non-dimensionalized by $u_\tau^*$, which is based on the sum of the two wall shear stresses at the suction and pressure walls. The linear profile is slightly distorted at the highest rotation number ($Ro_\tau$ = 15) giving a slope lower than twice the rotation speed and a shorter width of the linear profile, both of which indicate a tendency towards laminarization of the flow. The boundary layer thickens near the suction side at $y/\delta$ = 1 (hereafter, S. S.) and the velocity near the pressure side at $y/\delta$ = -1(P. S.) is slightly decreased.

In Cases SP & ST, no significant change but a little flattening of $U$ profiles appears. Noticeable shoulders are observed in Case ST as shown in Fig. 2(b). In these two cases, the mean velocity in the $z$-direction is induced due to the non-zero Coriolis force in that direction. Four zones of opposite motions are observed in Case ST with anti-symmetric profiles

around the channel centerline as shown in Fig 3(a). The corresponding profiles in Case WN are shown in Fig. 3(b), but they are similar to that of the fully developed two-dimensional channel flow. The magnitude of this velocity component increases with increasing $Ro_\tau$ so that the flow direction is tilted in the *z*-direction. Thus, in Cases ST & WN, the flow has three-dimensional characteristics, which are more pronounced in Case ST.

The mean flow angle $\gamma_m = \tan^{-1} W/U$ and the mean gradient angle $\gamma_g = \tan^{-1}(dW/dy/dU/dy)$ differ in Case ST and change their signs more drastically, while they have closer values in Case WN (El-Samni [7]). This implies that the flow in Case WN is closer to a 2-D turbulent channel flow. A measure of flow three-dimensionality is the structure parameter $a_1$ defined by the ratio of the vector magnitude of the shear stress to twice the turbulent kinetic energy, which is approximately constant at 0.15 in a 2DTBL [8]. Figure 4 shows typical profiles of $a_1$ in Cases ST & WN at the highest $Ro_\tau$ , where a significant distortion of $a_1$ in Case ST can be recognized. In Case WN, $a_1$ is much similar to that in the plane channel flow. This fact implies that the channel flow rotating around the wall-normal axis can be considered as a 2D flow tilted to the *z*-direction with an angle of $\gamma_m$ .

The friction coefficients normalized by the value of non-rotating channel are presented in Fig. 5, using the results of coarse-grid computations along with the values deduced from fine-grid simulation, which are denoted by larger symbols at only the highest $Ro_\tau$ in each case. Among the three studied cases, Case SP has distinguished behavior at each wall. Continuous suppression of the friction coefficient takes place on the S. S. wall. The value on the P. S. wall, however, shows non-monotonic behavior giving a peak near $Ro_\tau \approx 7.5$, beyond which continuous decrease appears indicating that increasing the rotation may lead to suppression of turbulence within the whole channel in this particular case. On the other hand the normalized $C_f$ in Cases ST & WN increases with increasing rotation in accordance with the velocity gradient observed in Fig. 2. It is noted from Fig. 5 that Case WN exhibits values of $C_f$ comparable to those of Case ST, although the rotation number is much lower. If the integral of the Coriolis term in the *x*-momentum equation, which is not zero in Case WN, is considered in the definition of $\tau_w$ , a larger value of normalized $C_f$ is obtained as shown in Fig. 5.

## TURBULENT INTENSITIES

The normal stresses normalized by $u_\tau^*$ in each rotation case are plotted along with those of non-rotating channel flow in Fig. 6. The superscript '*' has been omitted from the context for brevity. The profiles of normal stresses at a low $Ro_\tau$ of 2.5 [9] have been appended to trace the changes with the rotation number in Case SP. Much suppression at the suction side can be observed in all normal components. On the pressure side $\overline{uu}^*$ at $Ro_\tau$ = 15 reveals much suppression if compared with the augmentation in the other two components $\overline{vv}^*$ and $\overline{ww}^*$ . It should be noted that $\overline{vv}^*$ exceeds $\overline{uu}^*$ in the central region of the channel in Case SP.

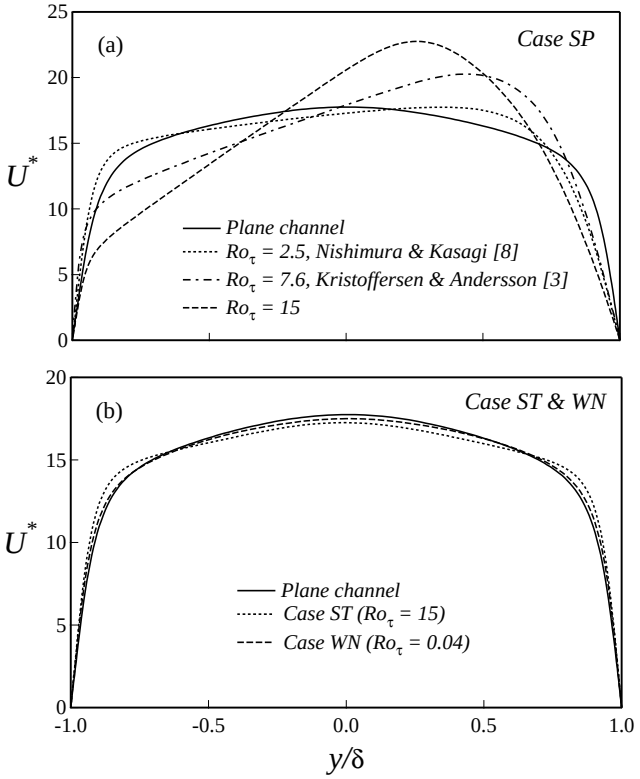


Figure 2 Mean velocity in *x*-direction: (a) Case SP; (b) Cases ST & WN

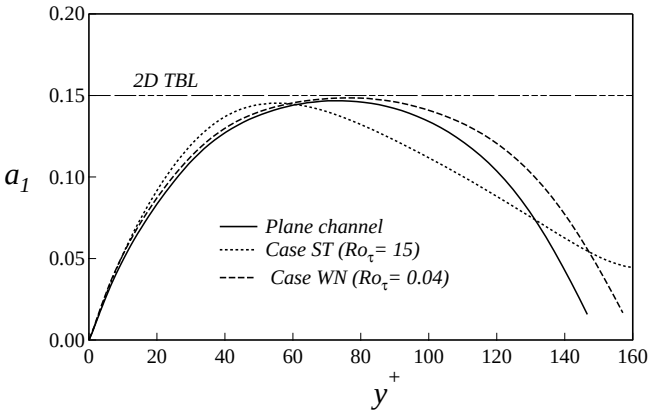


Figure 4 Structure parameter $a_1$ in Cases ST & WN.

In Case ST $\overline{uu}^*$ shows slight decrement than that of non-rotating channel near the walls associated with significant augmentation of $\overline{vv}^*$ and $\overline{ww}^*$ as shown in Fig. 6. Since no rotational production term for $\overline{uu}^*$ exists, this behavior can be attributed to the role, which the pressure-strain correlation plays in redistributing energy from $u$ to $v$ and $w$ components. The existence of various scales of eddies is in accordance with the enhancement of $v$ and $w$ components. In Case WN, all the normal stresses reveal augmentation especially $\overline{vv}^*$ and $\overline{ww}^*$, although the former has no rotational production term. In Fig. 6(c), $\overline{ww}^*$ shows sharp peak, which is similar to that of $\overline{uu}^*$. It can be concluded that the rotation has direct effect on modifying the normal stresses through the rotational production terms, while its indirect effect is clearly revealed in all rotation cases through modifying the pressure field and consequently on the pressure-strain correlations.

The Reynolds shear stress of $\overline{uv}^*$ in all studied orientations is plotted in Fig. 7, where the value of $Ro_\tau$ = 2.5 [8] is also appended. The non-monotonic behavior of normal stresses at the walls in Case SP is also observed in the trend of the shear stress $\overline{uv}^*$. Nearly zero values near the suction side can be observed at the $Ro_\tau$ = 15. The linear part of $\overline{uv}^*$ profile is shifted downwards at low-to-moderate $Ro_\tau$ before it goes up again beyond $Ro_\tau \sim 5$. This behavior was well addressed in [3] and can be attributed to the sign inversion of rotational production term in the transport equation of $\overline{uv}^*$, which is a function of ($\overline{uu}^* - \overline{vv}^*$). It can be seen from Fig. 6 that the rotational production term is negative at wide region of the channel, and this results in the reduced $\overline{uv}^*$. The sign remains positive in the vicinity of P. S., so that the peak of $\overline{uv}^*$ is shifted towards the wall.

In Cases ST & WN, $\overline{uv}^*$ is larger than the non-rotating case, which is attributed to the direct effect of the induced rotational production terms [7]. The off-diagonal components $\overline{uw}^*$ and $\overline{vw}^*$ are non-zeros in Cases ST & WN as shown in Fig. 8. It is worth mentioning that the rotational production terms in the transport equations of $\overline{uw}^*$ and $\overline{vw}^*$ play a key role in generating such stresses in Case ST. Such budgets would be of great help to improve current turbulence models,

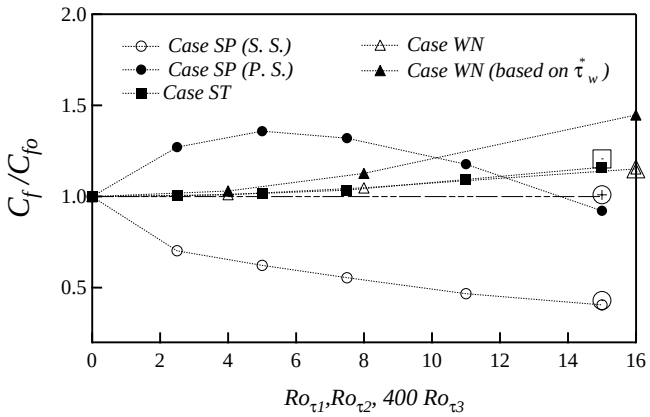


Figure 5 Normalized friction coefficients.

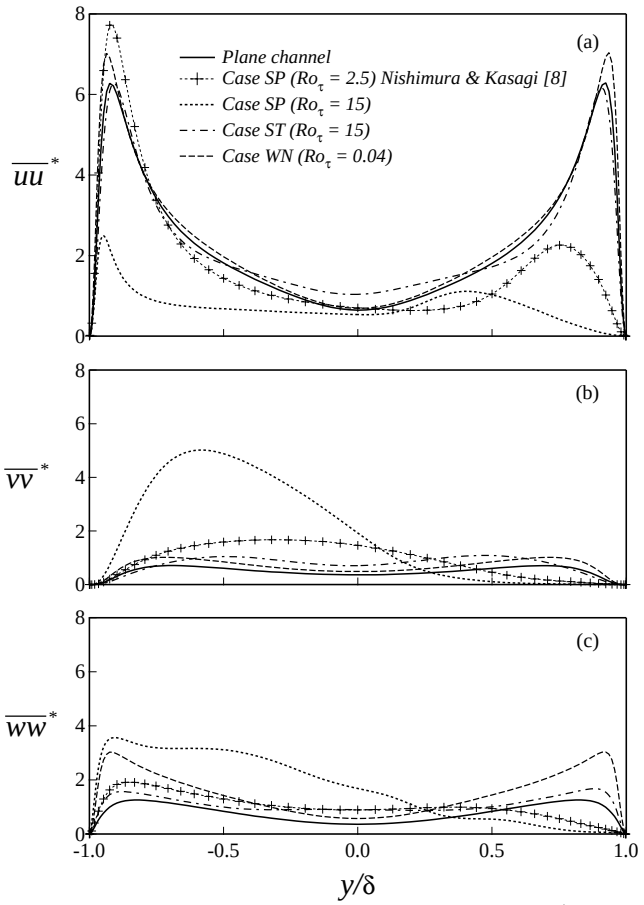


Figure 6 Normal stress in rotating channels: (a) $\overline{uu}^*$; (b) $\overline{vv}^*$; (c) $\overline{ww}^*$.

which fail to predict the off-diagonal stresses in the study of Oberlack et al. [5]. In Case WN, however, the rotational production terms are negligible due to the weak rotation numbers imposed in this case, and $\overline{uw}^*$ and $\overline{vw}^*$ profiles look like $\overline{uu}^*$ and $\overline{uv}^*$ in regular channel flow. A similarity was observed also in the budgets of the transport equations of both stresses. This suggests that Case WN can be regarded as a 2D channel flow with some tilting angle in the $z$-direction.

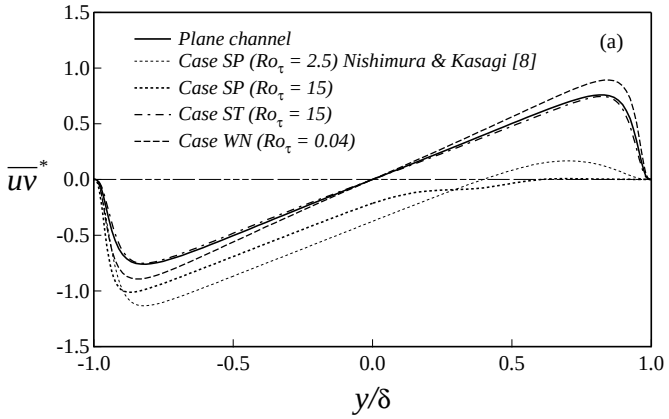


Figure 7 Reynolds shear stress of $\overline{uv}^*$.

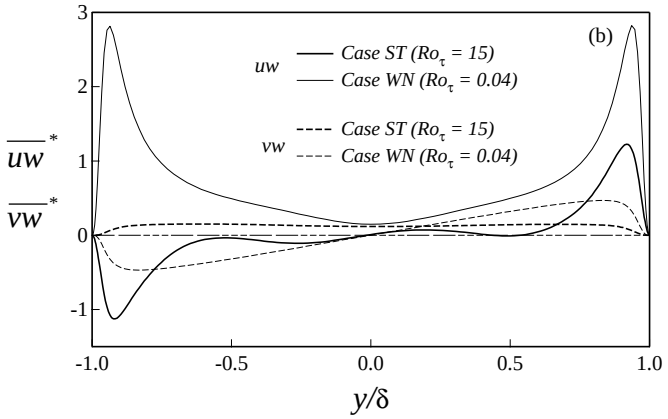


Figure 8 Reynolds shear stresses of $\overline{uw}^*$ and $\overline{vw}^*$.

## RMS VORTICITY

The vorticity dynamics have been addressed under the effect of different rotation orientations by tracing the RMSs of vorticity fluctuations and their budgets [7]. Presented here is the RMS of $\omega_x^+$ compared with that of the regular channel as shown in Fig. 9. Two peaks can be observed: one at the wall as a result of the opposite signed $\omega_x$ underneath the quasi-streamwise vortices and the other peak in the buffer layer due to the quasi-streamwise vortices. Although, the two peaks exist in regular channel their values and locations change in rotating channels. The rotational production term plays a direct role in increasing $\omega_x'$ in Case SP in the buffer layer. The plateau profile of $\omega_x'$ and the shifting of its peak further away from the wall suggest the existence of vortices of larger sizes occupying wider space in and out of the buffer layer. The peaks at the wall in Cases ST & WN are quite larger than that in regular channel due to the induced velocity $W$. The difference between the minimum and maximum peaks in the buffer layer diminishes in both cases. The distance between those two peaks, which can be roughly referred to the diameter of the vortices, is also decreasing. This may be attributed to the fewer number of vortices with slender diameters in Cases ST. However, in Case WN, this may be due to the fewer number of vortices aligned in the $x$-direction since the whole flow is tilted in the $z$-direction.

## BUDGETS

All terms in the transport equations of the relevant quantities to turbulence models have been calculated for the different rotation orientations studied. All components of Reynolds stresses, vorticity fluctuations, turbulent kinetic energy, and the dissipation rate of turbulent kinetic energy are of typical quantities beside other scalar related quantities. An example, shown in Fig. 10, is the turbulent kinetic energy $k$ normalized by the wall variables. Although no explicit dependence on the rotation number in the transport equation of $k$, drastical changes in the different terms in the budgets compared with the non-rotating case can be observed. Away

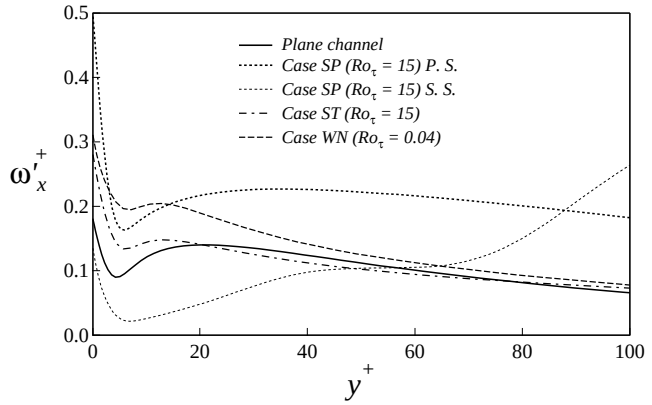


Figure 9 RMS vorticities normalized by local wall variables.

from the wall, the claim that $P_k = \varepsilon_k$ at $y^+ > 30$ does not hold satisfactorily in rotating flows. It can be shown that the turbulent transport $T_k$ becomes an important consuming term in Case SP (P. S.) but a producing term in Case ST. In the buffer layer, $T_k$ balances $P_k$ with larger contribution than $\varepsilon_k$ in these two cases. The pressure diffusion $\Pi_k$ reveals a dominant production effect in the viscous sublayer in Case SP, whereas it is of less importance in the other cases. The asymptotic values of $\varepsilon_k$ at the wall differ significantly in Cases SP and WN. The treatment of the modeled terms, $T_k$, $\Pi_k$ and $\varepsilon_k$ should be taken with caution when changing the rotation orientation.

## TURBULENT STRUCTURES

Visualization of the instantaneous flow fields is essential in discovering any change in turbulent structures when subjected to additional strains or body forces. Cross-stream vectors can give a picture about the vortical structures and large scale eddies as shown in Fig. 12. It should be mentioned that Kristoffersen and Andersson [3] observed large scale eddies of Taylor-Gortler types at low $Ro_\tau$ in Case SP. However, with increasing $Ro_\tau$ the persistence of the roll cells disappears and their sizes decrease. In Fig. 12 (a), at $Ro_\tau$ = 15, such roll cells disappear. Note that the top edge of Fig. 12(a) corresponds to the pressure side. Calm region of laminar

nature can be observed in the bottom edge of this figure. In Case ST, the fluid particles have the tendency to follow the background rotation, so that different sizes of eddy motions can be observed in Fig. 12 (b) and mostly that have a rotation sign same as the back ground rotation. Near the walls, the opposite motion of fluid particles is in accordance with the anti-symmetric profiles shown in Fig. 3(a).

For capturing the vortical structure in rotating channel flows, the negative second largest eigenvalue ( $\lambda_2$ ) of the tensor $S_{ik}S_{kj} + \Omega_{ik}\Omega_{kj}$ , used by Jeong et al. in plane channel flow [10], would be frame invariant and most suitable. RMS values of $\lambda_2$ are shown in Fig. 12, from which the threshold values in the visualizations are deduced. The figure shows a wide and plateau profile of $\lambda_2'$ in Case SP, which indicates the existence of slightly larger vortical structure at higher distances from the wall. In Case ST, $\lambda_2'$ has smaller peak than that in regular channel flow, indicating the existence of fewer number of structures. Case WN is much similar to plane channel although it gives slightly higher RMS value. This suggests the similarity between the plane channel and Case WN. In Fig. 13, the vortical structures in three cases are visualized with low- and high-speed streaks at a domain of $2.5\pi\delta \times \delta \times \pi\delta$ in all the studied cases. The planes of the low- and high-speed streaks lie at distances of around $y^+ \sim 12$. Vortices of longer extent in x-direction and larger sizes can be observed in Case SP (P. S.). Fewer number of vortices less-populated in Case ST is observed in Fig. 13(b), which may be attributed to the role the background rotation plays to boost the vortices rotating in the same direction and breaks down the vortices rotating in the opposite direction. In Case WN, most of the vortical structures are aligned in the tilted direction the same as the mean flow direction. Tilted streaks are observed in Cases ST & WN as shown in Fig. 13(b) & (c). T he streaks spacing in Case ST is around 270 viscous units, which is larger than that in regular channel flow. In Case WN, the spacing taken in a direction normal to the tilted streaks is closer to the 100 viscous units observed in plane channel flows in Kim et al.[11].

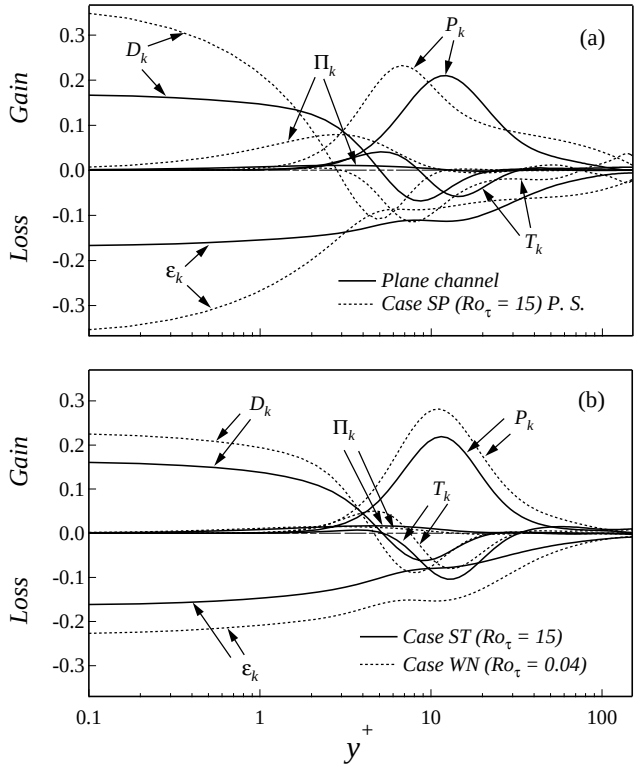


Figure 10 Terms in transport equation of turbulent kinetic energy: (a) non-rotating channel & Case SP; (b) Cases ST & WN.

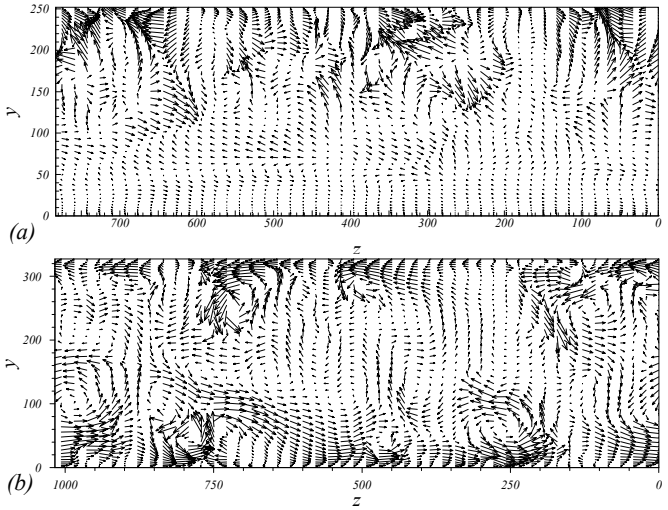


Figure 11 Instantaneous cross-streamwise velocity vectors at $Ro_\tau$ = 15: (a) Case SP; (b) Case ST.

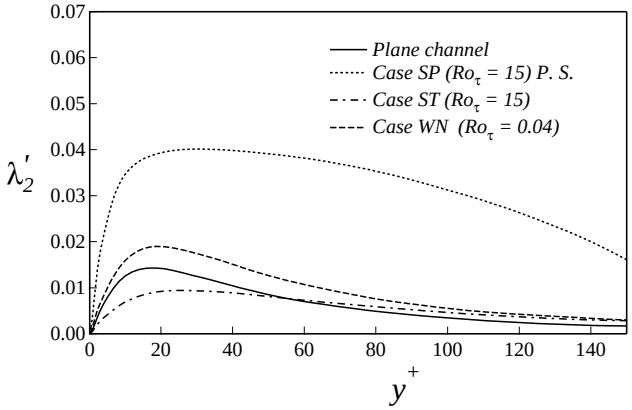


Figure 12 RMS values of $-\lambda_2$ in different rotating cases.

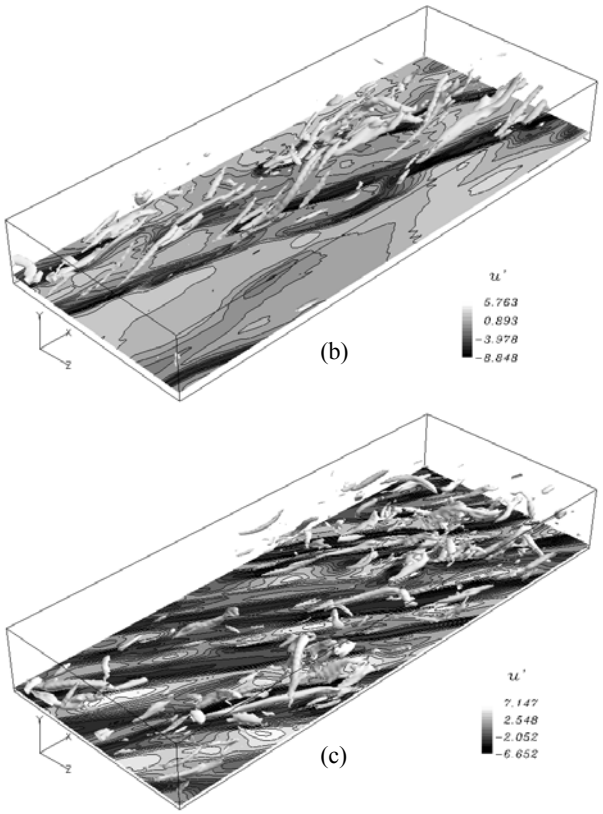


Figure 13 Vortical structures identified by $-\lambda_2$ embedded with the streaky structures in the near-wall region: (a) Case SP, $-\lambda_2 = 0.056$; (b) Case ST, $-\lambda_2 = 0.02$; (c) Case WN, $-\lambda_2 = 0.03$.

## CONCLUSIONS

Rotation orientation reveals different behavior of the statistical quantities as well as flow structures in turbulent channel flow. Laminarization in rotating channels takes place only near the leading side at moderate rotation numbers in Case SP. Increasing the rotation rate may lead to the laminarization of the whole flow. The linear profiles of the mean streamwise velocity are recaptured in Case SP for all the range of the rotation number, but with slight distortion at higher $Ro_\tau$ . Cases ST & WN exhibit more complicated flows. Three-dimensional flow characteristics can be deduced through the induced mean spanwise velocity and the generation of all Reynolds stress tensor components in both cases. The pressure-strain correlation plays a key role in redistributing energy from *u* to *v* and *w* components in rotating flows. It is shown that system rotation, when its axis is perpendicular to the mean flow vorticity, affects remarkably the mechanism of generating and sustaining the vortical structures near the wall. Those effects are evident in Cases ST & WN. Tilted streaky structures and less population of the vortical structures are observed in Case ST, whereas complicated structures aligned with the new mean flow direction are observed in Case WN. Case WN seems to be the most sensitive to system rotation among the cases studied, since it augments turbulence considerably at a rotation number two orders of magnitude smaller than those of Cases SP & ST. Databases for turbulence quantities and transport equations are generated

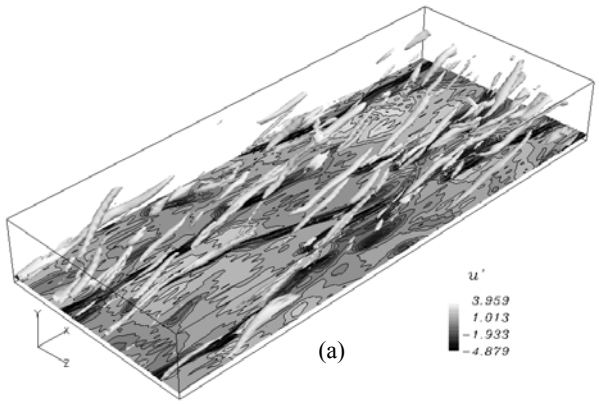


Figure 13 For caption, see the next page.

## ACKNOWLEDGMENTS

This numerical work is the results of "Micro Gas Turbine/Fuel Cell Hybrid-Type Distributed Energy System" which is supported by the Department of Core Research for Evolutional Science and Technology (CREST) of the Ministry of Education, Culture, Sports, Science and Technology (MEXT).

## REFERENCES

[1] Johnson, J. P., Halleen, R. M. and Lezius, D. K., 1972, "Effects of Spanwise Rotation on The Structure of Two-Dimensional Fully Developed Turbulent Channel Flow," *J. Fluid Mech.*, **56**, pp. 533-557.

[2] Kim, J., 1983, "The Effect of Rotation on Turbulence Structure," *In Proc. of 4th Symp. on Turbulent Shear Flows*, Karlsruhe pp. 6.14-6.19.

[3] Kristoffersen, R. and Andersson, H. I., 1993, "Direct Simulations of Low Reynolds-Number Turbulent Flow in a Rotating Channel," *J. Fluid Mech.*, **256**, pp. 163-197.

[4] Andersson, H. I. and Kristoffersen, R., 1995, "Turbulence Statistics of Rotating Channel Flow," *In the Proc. of 9th Symp. on Turbulent Shear Flows*, Kyoto, Japan, pp. 53-70.

[5] Oberlack, M., Cabot, W. & Rogers, M. M., 1999, "Turbulent Channel Flow with Streamwise Rotation: Lie Group Analysis, DNS and Modelling," *In the 1st int. Symp. in Turbulence and Shear Flow Phenomena*, USA, pp. 85-90.

[6] Fukunaga, S., Uechi, H. & Kasagi, N., 2000, "Development of GUI Software for Cycle Analysis and Conceptual Design of Micro Gas Turbine," (in Japanese), *Proc. 28th Gas Turbine Conf.*, Tokyo, 2000, pp. 141-146.

[7] El-Samni, O., 2001, "Heat and Momentum Transfer in Turbulent Rotating Channel Flow," Ph. D. thesis. The University of Tokyo, Tokyo, Japan.

[8] Sendstad, O. & Moin, P., 1992, "The Near-Wall Mechanics of Three-Dimensional Turbulent Boundary Layers," Stanford University, Dept. Mech. Eng., Thermosciences Div. Rep. TF-57.

[9] Nishimura, M. and Kasagi, N., 1996, "Direct Numerical Simulation of Combined and Natural Turbulent Convection in a Rotating Plane Channel," *Proc. of 3rd KSME-JSME, Thermal Engineering Conference*, Korea, Vol. 3, pp. 77-82.

[10] Jeong, J., Hussain, F., Schoppa, W. & Kim, J., 1997, " Coherent Structures Near the Wall in a Turbulent Channel Flow," *J. Fluid Mech*. **332**, pp.185-214.

[11] Kim, J., Moin, P. & Moser, R., 1987, "Turbulence Statistics in Fully Developed Channel Flow at Low Reynolds Number," *J. Fluid Mech*. **177**, pp.133-166.